AIP | The Journal of Chemical Physics

The nature of singlet excitons in oligoacene molecular crystals

H. Yamagata, J. Norton, E. Hontz, Y. Olivier, D. Beljonne et al.

Citation: J. Chem. Phys. **134**, 204703 (2011); doi: 10.1063/1.3590871
View online: http://dx.doi.org/10.1063/1.3590871
View Table of Contents: http://jcp.aip.org/resource/1/JCPSA6/v134/i20
Published by the American Institute of Physics.

The nature of singlet excitons in oligoacene molecular crystals

H. Yamagata,[1] J. Norton,[2] E. Hontz,[1] Y. Olivier,[3] D. Beljonne,[3] J. L. Brédas,[2] R. J. Silbey,[4] and F. C. Spano[1,a)]

[1]*Department of Chemistry, Temple University, Philadelphia, Pennsylvania 19122, USA*
[2]*School of Chemistry and Biochemistry and Center for Organic Photonics and Electronics, Georgia Institute of Technology, Atlanta, Georgia 30332-0400, USA*
[3]*Laboratory for Chemistry of Novel Materials, University of Mons, Place du Parc 20, B-7000 Mons, Belgium*
[4]*Department of Chemistry and Center for Excitonics, Massachusetts Institute of Technology, Cambridge, Massachusetts 02139, USA*

(Received 6 January 2011; accepted 25 April 2011; published online 26 May 2011)

A theory for polarized absorption in crystalline oligoacenes is presented, which includes Frenkel exciton coupling, the coupling between Frenkel and charge-transfer (CT) excitons, and the coupling of all neutral and ionic excited states to the dominant ring-breathing vibrational mode. For tetracene, spectra calculated using all Frenkel couplings among the five lowest energy molecular singlet states predict a Davydov splitting (DS) of the lowest energy (0–0) vibronic band of only -32 cm^{-1}, far smaller than the measured value of 631 cm^{-1} and of the wrong sign—a negative sign indicating that the polarizations of the lower and upper Davydov components are reversed from experiment. Inclusion of Frenkel-CT coupling dramatically improves the agreement with experiment, yielding a 0–0 DS of 601 cm^{-1} and a nearly quantitative reproduction of the relative spectral intensities of the 0–*n* vibronic components. Our analysis also shows that CT mixing increases with the size of the oligoacenes. We discuss the implications of these results on exciton dissociation and transport. © *2011 American Institute of Physics*. [doi:10.1063/1.3590871]

I. INTRODUCTION

Oligoacenes and their derivatives are prominent organic semiconductors.[1–3] High charge-carrier mobilities have been reported in pentacene, tetracene, and rubrene (a tetraphenyl-substituted tetracene derivative), generating marked interest for applications in field-effect transistors.[4–7] In contrast to the conventional wisdom that molecular order and tight packing are detrimental to luminescence in organic crystals, emission from the lowest singlet exciton in anthracene[8] and tetracene[9–12] thin films is allowed and even coherently enhanced at low temperatures, leading to superradiance. Efficient molecular-based photovoltaic cells based on pentacene/C_{60} heterojunction or bi-layer devices have been fabricated;[13,14] modeling of these devices yields pentacene singlet exciton diffusion lengths in excess of 65 nm and nearly quantitative exciton-to-charge conversion efficiency.

In the present work, we seek to provide a better understanding of the oligoacene photophysical properties by addressing the nature of the lowest singlet excitons. We do so by re-examining the Davydov splitting (DS) (Ref. 15) in the absorption spectrum of oligoacene crystals. The presence of two non-equivalent molecules per unit cell in these crystals results in two optical transitions that are mainly polarized along the two directions ($||b$ and $\perp b$) of the herringbone *ab* plane. The DS for excitation normal to the *ab* plane ranges from $\sim$200 cm^{-1} in anthracene[16,17] to $\sim$630 cm^{-1} in tetracene[18,19] and $\sim$1100 cm^{-1} in pentacene [20,21] for the lowest vibronic (0–0) transition. An extensive analysis of the Davydov splitting in oligoacenes was conducted earlier by Schlosser and Philpott, who concluded that fair agreement with experiment could be obtained only when including higher-lying Frenkel (i.e., molecular) excitations for tetracene and pentacene.[22] However, Schuster *et al.*[23], using inelastic electron scattering on pentacene crystals, demonstrated the inability of a purely Frenkel exciton model to account for the exciton dispersion; these authors suggested the need to include coupling to intermolecular charge-transfer (CT) excitons. In crystalline oligoacenes, the existence of CT excited states has been shown early on by Sebastian *et al.* [24,25] via electro-absorption experiments and, much more recently, by Zhu and co-workers through time- and angle-resolved two-photon photoemission spectroscopy.[26,27] A strong CT contribution to the DS of tetracene was, in fact, suggested by the theoretical work of Petelenz *et al.*[28] in the late 1980s. A more recent theoretical analysis for pentacene by Tiago *et al.*[29] also showed the importance of CT to the DS. However, neither Ref. 28 nor Ref. 29 incorporated vibronic coupling, which has a major impact on the Davydov splitting.[30] Hence, a more quantitative estimate of the relative contribution from CT excitations into the lowest singlet excitons and their impact on the DS have remained elusive; this was due to the lack of a theoretical model that could quantitatively account for: (i) excitonic interactions among Frenkel states; (ii) mixing between Frenkel excitons and charge-transfer pairs; and (iii) coupling of both Frenkel and CT excitations to molecular vibrations, all on an *equal* footing. The present work intends to fill this gap by employing a multi-band Holstein-like Hamiltonian represented within the one- and two-particle basis.[31–36] This approach provides an essentially exact treatment of vibronic coupling in the absorpion and emission spectra of Frenkel excitons.[32,36]

a)Electronic mail: spano@temple.edu.

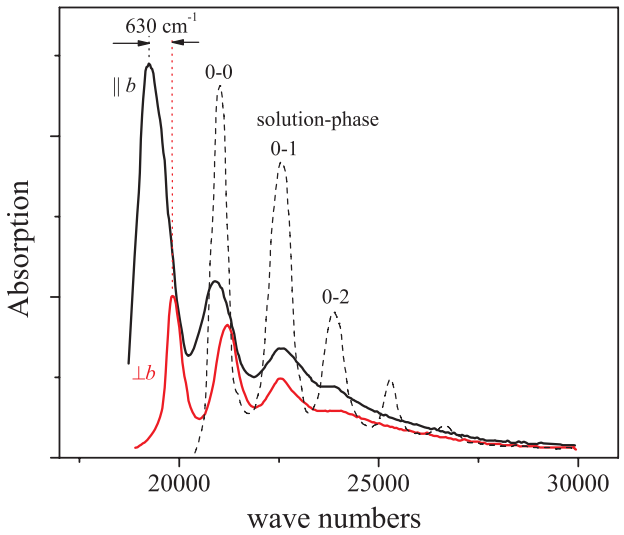

FIG. 1. Tetracene solution-phase and crystal absorption spectra reproduced from Bree and Lyons (see Ref. 18). The crystal spectra correspond to excitation normal to the *ab* plane. The Davydov splitting of the 0–0 transition is indicated.

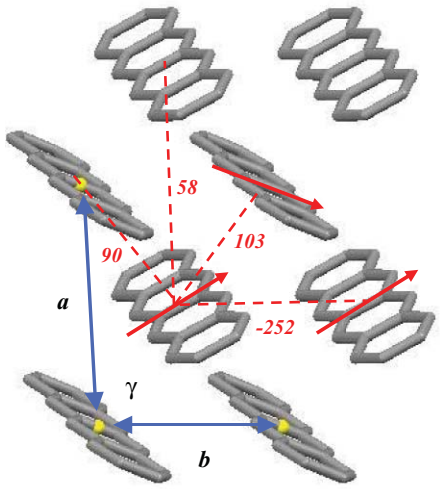

FIG. 2. Section of the *ab* plane in crystalline tetracene. The red arrows denote the polarization of the lowest molecular ($S_0 \rightarrow S_1$) electronic transition. Since the unit cell for tetracene (and pentacene) is triclinic the *a* and *b* axes are not orthogonal ($\gamma = 94°$). Because there is no symmetry operation relating to the two molecules in the unit cell the optical transitions defining the two Davydov components are mainly, but not entirely, polarized along *b* and normal to *b*. (By contrast, for the monoclinic unit describing crystalline anthracene, the optical transitions are polarized exactly along the unique *b* axis and normal to *b*.) Note that our definition of the *b*-axis is that which contains the *nearest* equivalent neighbors, ($b = 6.06$ Å) consistent with Bree and Lyons (see Ref. 18). The figure also shows calculated unscreened excitonic couplings involving only the S_1 state in units of cm^{-1}. The center of inversion located at the molecular centers can be used to evaluate the remaining near neighbor interactions. Couplings for the other sublattice are similar but not identical.

In what follows, we first conduct a comprehensive analysis of the polarized absorption spectrum of triclinic tetracene crystals measured by Bree and Lyons[18] and more recently by Tavazzi *et al.*[19] In contrast to all previous works, we attempt to reproduce not only the 630 cm^{-1} DS of the 0-0 component of the lowest energy, short-axis polarized optical transition but also the splittings of all higher-energy ($0 \rightarrow 1$, $0 \rightarrow 2$, ...) vibronic bands, as well as the relative band intensities for each polarization component. The impact of intermolecular interactions on the absorption and emission vibronic band intensities has been shown to yield important information about exciton bandwidth and the nature of disorder.[32–34] We further evaluate the Davydov splitting in antracene and pentacene, showing that the CT character of the lowest energy exciton increases significantly with oligomer length. Finally, we investigate the impact of CT/Frenkel mixing on the exciton dispersion and the derived diffusion coefficients.

II. DAVYDOV SPLITTING IN TETRACENE

Before discussing our calculations, it is useful to recall what is known experimentally about the impact of crystallization on the absorption spectrum of tetracene. Figure 1 shows the measured solution-phase absorption spectrum of tetracene as well as the polarized absorption spectrum of the crystal in the vicinity of the lowest optical transition, as measured by Bree and Lyons.[18] The solution-phase spectrum displays a clear vibronic progression of the symmetric breathing mode with energy $\hbar\omega_0 = 1430$ cm^{-1}, with an approximate Huang-Rhys factor of unity (as determined by comparing the 0–0 and 0–1 spectral *areas*).

In the crystal phase, molecules are arranged in a triclinic Bravais lattice with two molecules per unit cell, as indicated in Fig. 2. The spectra in Fig. 1 show that in the crystal phase, the absorption spectrum becomes dependent on the polarization of the exciting light. In particular, the 0–0 transition undergoes a more significant redshift when the excitation electric field is along the crystallographic *b* axis, compared to when the electric field is normal to the *b*-axis. This leads to a substantial DS of ~630 cm^{-1} for the 0–0 component as indicated in the figure, and about half that value for the 0–1 component. Overall, the *b*-polarized vibronic progression shows the greatest deviation relative to the solution-phase spectrum, with namely a much larger 0–0 to 0–1 oscillator strength ratio, $A^{0-0}_{||b}/A^{0-1}_{||b}$ (roughly twice as large as the solution phase value of approximately unity). In contrast, the component of the absorption spectrum polarized perpendicular to *b* is not significantly changed compared with the solution spectrum (except for extra broadening and an overall solution-to-crystal redshift).

A. Frenkel-Holstein model

In an initial effort to understand the impact of aggregation on the tetracene absorption spectrum, we employ a multi-band Frenkel exciton model with linear exciton vibrational coupling. The model incorporates five Frenkel exciton bands derived from the lowest five excited singlet states in tetracene (S_1–S_5) and their couplings to the dispersionless optical phonons originating from the ≈ 1430 cm^{-1} ring breathing mode. The multi-band Frenkel-Holstein

Hamiltonian is

$$H_{FE} = \sum_{\sigma}\sum_{\boldsymbol{n}\in\sigma}\sum_{i=1,5}(\omega^{i}_{0-0}+\Delta_{0-0})\,|\boldsymbol{n},i\rangle\,\langle\boldsymbol{n},i| + \sum_{\sigma,\sigma'}\sum_{\boldsymbol{n}\in\sigma,\boldsymbol{m}\in\sigma'}\sum_{i,i'}\boldsymbol{J}^{ii'}_{\boldsymbol{nm}}\,|\boldsymbol{n},i\rangle\langle\boldsymbol{m},i'| + \omega_0\sum_{\sigma}\sum_{\boldsymbol{n}\in\sigma} b^{\dagger}_{\boldsymbol{n}}b_{\boldsymbol{n}} + \omega_0\sum_{\sigma}\sum_{\boldsymbol{n}\in\sigma}\sum_{i=1,5}\{\lambda_i(b^{\dagger}_{\boldsymbol{n}}+b_{\boldsymbol{n}})+\lambda_i^2\}\,|\boldsymbol{n},i\rangle\,\langle\boldsymbol{n},i|\,, \tag{1}$$

where we have taken $\hbar = 1$. The first two terms in Eq. (1) comprise the usual Frenkel exciton Hamiltonian generalized for the five bands. The sum over all molecules is accomplished in two stages: first a sum over all equivalent molecules with a given sublattice σ, followed by a sum over the two sublattices ($\sigma = 1, 2$). The state $|\boldsymbol{n}, i\rangle$ represents a pure electronic excitation in the singlet state S_i on molecule $\boldsymbol{n}$ with all other molecules in their electronic ground states (S_0). The transition energies corresponding to the five molecular excitations, ω^{i}_{0-0} (i = 1–5), are taken from measurements in solution (see the Appendix for all molecular parameters). The solution-to-crystal shift Δ_{0-0}, arising from nonresonant dispersion interactions, is assumed uniform for all excitations.

The second term in Eq. (1) contains the excitonic couplings, $\boldsymbol{J}^{ii'}_{\boldsymbol{nm}} \equiv \langle \boldsymbol{n}, i|H|\boldsymbol{m}, i'\rangle$, evaluated using the INDO/CSSD molecular transition densities associated with the singlet states S_i and $S_{i'}$. After the molecular transition densities were expanded as atomic monopoles the excitonic couplings were calculated from atom-atom Coulombic sums between interacting molecules, as described in previous studies.[37–39] The excitonic couplings $J^{ii'}_{\boldsymbol{nm}}$ were also scaled by the transition dipole moment ratio $\mu_{i,\mathrm{exp}}\mu_{i',\mathrm{exp}}/\mu_i\mu_{i'}$, as was done by Schlosser and Philpott,[22] to obtain more reliable results. Experimental transition dipoles are reported in Table VI.

The third term in Eq. (1) represents the vibrational energy of the symmetric stretching mode with frequency, $\omega_0 = 0.18$ eV (1430 cm^{-1}). $b^{\dagger}_n$ (b_n) creates (destroys) a vibrational quantum in the unshifted (S_0) ground state nuclear potential well on molecule $\boldsymbol{n}$. The final term in Eq. (1) accounts for the linear exciton-vibrational coupling. λ_i^2 is the Huang-Rhys (HR) factor which measures the shift of the S_i excited state potential relative to S_0. In all that follows we set $\lambda^2_{i=1} = 1$ for the lowest excited state and $\lambda^2_{i>1} = 0$ for all higher excited states. The latter approximation is quite good since the high energy states (S_2–S_5) are separated from S_1 by energies much greater than a vibrational quantum.

The Hamiltonian in Eq. (1) is represented in a delocalized basis set including one- and two-particle states.[31,32,35] Accordingly, the αth eigenstate with wave vector $\boldsymbol{k}$ is expanded as

$$|\Psi_{\alpha,k}\rangle = \sum_{\sigma}\sum_{i=1,5}\sum_{\tilde{v}_i=0,1,\ldots5} c^{\alpha,\boldsymbol{k}\sigma}_{i,\tilde{v}_i}\,|\boldsymbol{k}\sigma,i,\tilde{v}_i\rangle + \sum_{\sigma}\sum_{i=1,5}\sum_{\substack{\tilde{v}_i=0,1,\ldots4\\ v=1,\ldots4}}\sum_{\boldsymbol{l}} c^{\alpha,\boldsymbol{k}\sigma}_{i,\tilde{v}_i;\boldsymbol{l},v}\,|\boldsymbol{k}\sigma,i,\tilde{v}_i;\ \boldsymbol{l},v\rangle\,. \tag{2}$$

Here, we have introduced the delocalized one-particle Frenkel excitons with wave vector $\boldsymbol{k}$ on sublattice σ,

$$|\boldsymbol{k}\sigma,i,\tilde{v}_i\rangle = \frac{1}{\sqrt{N_{cell}}}\sum_{\boldsymbol{n}\in\sigma} e^{i\boldsymbol{k}\cdot\boldsymbol{n}}\,|\boldsymbol{n},i,\tilde{v}_i\rangle\,, \quad \sigma = 1,\ 2;\quad i\ =\ 1,\ 2,\ldots5, \tag{3}$$

and the two-particle excitons with wave vector $\boldsymbol{k}$ and separation $\boldsymbol{l}$ on sublattice σ,[32,33]

$$|\boldsymbol{k}\sigma,i,\tilde{v}_i;\boldsymbol{l},v\rangle = \frac{1}{\sqrt{N_{cell}}}\sum_{\boldsymbol{n}\in\sigma} e^{i\boldsymbol{k}\cdot\boldsymbol{n}}\,|\boldsymbol{n},i,\tilde{v}_i;\ \boldsymbol{n}+\boldsymbol{l},v\rangle, \quad \sigma = 1,\ 2;\ \ i\ =\ 1,\ 2,\ldots5. \tag{4}$$

Local one-particle states in Eq. (3) are represented as $|\boldsymbol{n}, i, \tilde{v}_i\rangle$ where $\tilde{v}_i$ is the number of excited state vibrational quanta in the (shifted) nuclear potential of the excited state S_i for a molecule at position $\boldsymbol{n}$. All other molecules are in their vibrationless ground state (S_0). The local two-particle states, $|\boldsymbol{n}, i, \tilde{v}_i;\ \boldsymbol{n}+\boldsymbol{l}, v\rangle$ ($v \geq 1$), in Eq. (4) consist of a vibronic/vibration pair; in addition to the vibronic excitation at site $\boldsymbol{n}$, there is a purely vibrational excitation within the ground state (S_0) nuclear potential at site $\boldsymbol{n}+\boldsymbol{l}$. The two-particle states are directly responsible for establishing the (excitonic) polaron radius.[40]

For excitation along (001) Philpott showed that the crystal Davydov splitting in polyacenes can be accurately calculated by performing interaction sums over a single *ab* (herringbone) plane.[41] Hence, in all that follows we assume excitation along (001) and model the crystal response with a single *ab* layer (see Fig. 2). Once expressed in the basis set defined above, we numerically diagonalize the Hamiltonian to determine all eigenstates and energies for a square herringbone aggregate in the *ab* plane. In our calculations, we limited the two-particle states to those with vibronic-vibrational separations less than 10 Å , which reduce the basis set to a manageable size without sacrificing accuracy. We confirmed that doubling the radius to 20 Å had negligible effect on the calculated spectra. In addition, we capped the total number of vibrational quanta in the one and two-particle states at five.

After checking that the 2D lattice sums reproduced the results of Ref. 22 in the point dipole approximation, we used the more quantitative quantum-chemical excitonic couplings $\boldsymbol{J}^{ii'}_{\boldsymbol{nm}}$ to simulate the absorption spectrum of a large (300 × 300) tetracene *ab* lattice for excitation normal to the *ab* plane. To evaluate the absorption spectrum for light polarized in the direction $\boldsymbol{j}$ (= *a,b*) we used the expression,

$$A_j(\omega) = \sum_{\alpha}|\langle G|\hat{\boldsymbol{\mu}}\cdot\boldsymbol{j}|\Psi_{\alpha,\boldsymbol{k}=0}\rangle|^2 W_{LS}(\omega-\omega_{\alpha,\boldsymbol{k}=0}), \tag{5}$$

where $|G\rangle = |g\rangle\otimes|vac\rangle$is the vibrationless ground state of the aggregate, consisting of the product of $|g\rangle$, the pure electronic ground state (all molecules in S_0), and $|vac\rangle$, the vacuum state of all vibrations within the S_0 nuclear well. $\omega_{\alpha,\boldsymbol{k}=0}$ is the transition energy of the αth eigenstate with wave vector $\boldsymbol{k} = 0$, and $\hat{\mu}$ is the aggregate transition dipole moment operator,

$$\hat{\boldsymbol{\mu}} \equiv \sum_{i=1,\ldots,5}\sum_{\sigma}\sum_{\boldsymbol{n}\in\sigma}\boldsymbol{\mu}_i|g\rangle\langle\boldsymbol{n},i| + \mathrm{h.c.}, \tag{6}$$

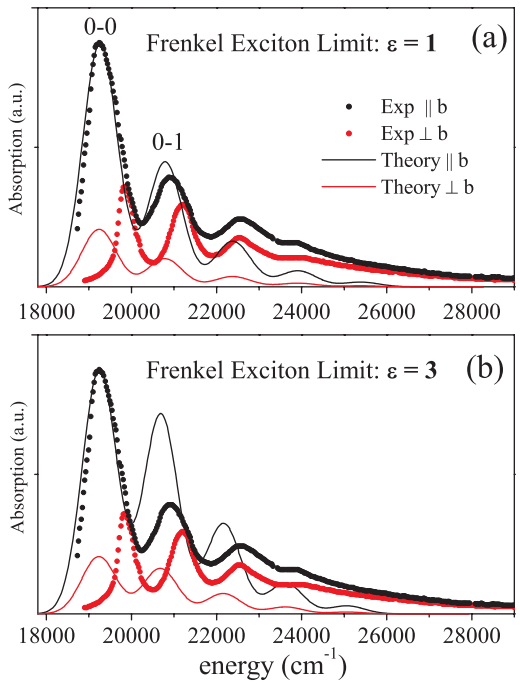

FIG. 3. Polarized absorption spectrum for crystalline tetracene calculated on the basis of a purely Frenkel exciton model alongside the measured spectra of Bree and Lyons (see Ref. 18). In (a) the unscreened INDO/CCDSD evaluated couplings are employed. In (b) the couplings are divided by ε. Calculated spectra are spectrally shifted so that the *b*-polarized 0–0 peak frequency agrees with experiment (by adjusting the spectral shift Δ_{0-0}); in addition, calculated spectra are normalized to the experimental 0–0 peak intensity for the component polarized along *b*.

where $\boldsymbol{\mu}_i$ is the molecular dipole moment corresponding to the $S_0 \rightarrow S_i$ transition. In all calculations presented in this work we incorporate the measured solution-phase transition dipole moments (see the Appendix). Finally, W_{LS} in Eq. (5) is a line shape function, chosen here to be Gaussian, $W_{LS}(\omega) = \exp(-\omega^2/\sigma_L^2)$, with a 1/e full-width of $2\sigma_L$.

Our calculated spectra appear in Fig. 3 alongside the measured spectra of Bree and Lyons.[18] We utilized two different values of dielectric constant ε; $\varepsilon = 1$, in which interactions are entirely unscreened, and $\varepsilon = 3$, which corresponds to the measured value of the square of isotropically averaged refractive index.[42] To incorporate screening, all Frenkel couplings are reduced by ε. Figure 3 shows that the spectrum using unscreened interactions agrees reasonably well with experiment for the vibronic peak ratio $A_{||b}^{0-0}/A_{||b}^{0-1}$, but completely fails to reproduce the Davydov splittings for all 0-*n* transitions. When screened interactions are used both the spectral intensities and splittings are in poor agreement with experiment. The most egregious disparity in both cases corresponds to the calculation of a small DS value for the 0–0 transition of only -32 cm^{-1} (unscreened) and -10 cm^{-1} (screened), far smaller than the measured value of 630 cm^{-1}. Here, we define the DS to be the difference between the peak frequency of the component perpendicular to *b* and that polarized along *b*. Hence, a negative DS value indicates that the calculated lower and upper Davydov components have polarizations that are reversed from what is observed, i.e., the lower Davydov component is polarized mainly along a direction perpendicular to *b*.

The negative DS in Fig. 3 can be easily rationalized within a simple model where only the lowest energy Frenkel excited state per molecule is retained, vibronic coupling is ignored, and a monoclinic unit cell is assumed. In this case, the symmetric and antisymmetric combinations of the S_1 molecular states yield two excitonic bands with respective dispersions, $L_{11}(\boldsymbol{k}) + L_{12}(\boldsymbol{k})$ and $L_{11}(\boldsymbol{k}) - L_{12}(\boldsymbol{k})$, fixed by the electronic couplings between equivalent molecules within a given sublattice,[3,15]

$$L_{11}(\boldsymbol{k}) \equiv (1/N_{cell}) \sum_{\boldsymbol{m}\in''1'',\boldsymbol{n}\in''1''} \boldsymbol{J}_{\boldsymbol{mn}}^{11} \exp[i\boldsymbol{k}\cdot(\boldsymbol{m}-\boldsymbol{n})], \tag{7}$$

as well as interactions between non-equivalent molecules in different sublattices,

$$L_{12}(\boldsymbol{k}) \equiv (1/N_{cell}) \sum_{\boldsymbol{m}\in''1'',\boldsymbol{n}\in''2''} J_{\boldsymbol{mn}}^{11} \exp[i\boldsymbol{k}\cdot(\boldsymbol{m}-\boldsymbol{n})]. \tag{8}$$

The Davydov splitting depends only on the interaction between the two lattices and is given by $-2L_{12}(0)$, in accord with our adopted sign convention. Our quantum mechanical calculations yield a large and negative value for $L_{11}(0)$ (≈ -700 cm^{-1}) so that both sub-lattices behave as massive J-aggregates (which is the source of the superradiance effect), yet a smaller and *positive* value for $L_{12}(0)$ ($\approx$ 70 cm^{-1}), which *raises* the symmetric *b*-polarized Davydov component 140 cm^{-1} *higher* in energy than its antisymmetric (*a*-polarized) counterpart. Increasing the number of Frenkel exciton bands and activating vibronic coupling further reduces the magnitude of the DS but does not change its sign, as shown in Fig. 3. The same trend is also obtained when increasing the dielectric constant in the range 1–3.[43]

B. Coupling to charge transfer excitons

The same analysis for the tetracene absorption spectrum was then repeated while explicitly including charged molecular pairs in the model. The relative energies of the CT excitations are fixed by the measured 0.35 eV gap between the lowest CT state (located on nearest-neighbor molecules) and the lower 0–0 Davydov component, as obtained from the electro-absorption experiments of Sebastian *et al.*[25] The Hamiltonian matrix elements mixing Frenkel and CT excitations are expressed in terms of hole and electron transfer integrals computed at the density functional theory level. Finally, the electron-phonon coupling between CT excitons and the high-frequency vibration is modeled using cation and anion HR factors, with the former derived from the ultraviolet photoelectron spectrum of gas-phase tetracene and the latter derived from density functional theory (DFT) calculations.[44]

The total Hamiltonian is expressed as

$$H = H_{FE} + H_{CT} + H_{CTV}, \tag{9}$$

where H_{FE} was defined already in Eq. (1), H_{CT} represents the energy of the charge-separated states along with their coupling to the neutral Frenkel excitations and H_{CTV} accounts for the linear exciton-vibrational coupling between the CT states

TABLE I. CT state energies (in cm^{-1}) for tetracene derived from the measured electroabsorption spectra (Ref. 25) relative to the lowest molecular exciton (S_1) energy. Also shown are the calculated dissociation integrals.

Tetracene l	$\omega_{0-0}^{CT}(\boldsymbol{l}) - (\omega_{0-0}^{i=1} + \Delta_{0-0})$	$D_h(\boldsymbol{l})$	$D_e(\boldsymbol{l})$
(1/2, 1/2)	x	203.3	583.2
(−1/2, 1/2)	x	− 609.8	− 563.8
(0,1)	$x + 557$	26.6	− 122.6
(1,0)	$x + 1492$	− 0.8	− 8.1

$x = 1334$ ($\varepsilon = 1$), 1620 ($\varepsilon = 2$), and 1695 ($\varepsilon = 3$)

and the symmetric vibrational mode. H_{CT} takes the form

$$H_{CT} = \sum_{\sigma,\boldsymbol{n}\in\sigma,l} \omega_{0-0}^{CT}(\boldsymbol{l}) \,|\boldsymbol{n},+;\boldsymbol{n}+\boldsymbol{l},-\rangle\langle\boldsymbol{n},+;\boldsymbol{n}+\boldsymbol{l},-| + \sum_{\sigma,\boldsymbol{n}\in\sigma,l} \{D_e(\boldsymbol{l})\,|\boldsymbol{n},1\rangle\langle\boldsymbol{n},+;\ \boldsymbol{n}+\boldsymbol{l},-| + D_h(\boldsymbol{l})\,|\boldsymbol{n},1\rangle\langle\boldsymbol{n}+\boldsymbol{l},+;\ \boldsymbol{n},-|\} + h.c. \quad (10)$$

The pure electronic state $|\boldsymbol{n},+;\ \boldsymbol{n}+\boldsymbol{l},-\rangle$ represents a cation/anion pair at $\boldsymbol{n}$ and $\boldsymbol{n}+\boldsymbol{l}$. (Note that the state $|\boldsymbol{n},-;\ \boldsymbol{n}+\boldsymbol{l},+\rangle$ is equivalent to $|\boldsymbol{n}+\boldsymbol{l},+;\ \boldsymbol{n},-\rangle$.) $\omega_{0-0}^{CT}(\boldsymbol{l})$is the energy of the CT pair in which the ions are separated by $\boldsymbol{l}$. The energies of the charge separated states relative to the lowest singlet Frenkel exciton ($\|b$ 0–0 absorption peak) have been measured for anthracene, tetracene, and pentacene in the electro-absorption experiments of Sebastian *et al.*[24,25] and are, respectively, 0.43 eV, 0.35 eV, and 0.29 eV. Table I contains the CT energies, $\omega_{0-0}^{CT}(\boldsymbol{l})$, (relative to $\omega_{0-0}^{i=1} + \Delta_{0-0}$) obtained by adjusting $\omega_{0-0}^{CT}(\boldsymbol{l} = (1/2, 1/2))$ in our calculations until the spectral separation between the nearest-neighbor CT state and the lowest Frenkel exciton matched the measured value of 0.35 eV. The Hamiltonian in Eq. (9) considers only the ionization of the lowest energy exciton as we are most interested in the optical properties near the band bottom. Ionization of higher excitons would not directly impact the low-energy band structure, but would be required to understand optical charge generation.[45]

The Frenkel exciton dissociation integrals appearing in Eq. (10) are assumed to depend only on $\boldsymbol{l}$ and are approximately related to the electron and hole resonance integrals by

$$D_e(\boldsymbol{l}) = t_{\mathrm{LUMO}}(\boldsymbol{l}), \quad (11a)$$

and

$$D_h(\boldsymbol{l}) = -t_{\mathrm{HOMO}}(\boldsymbol{l}). \quad (11b)$$

Here, the resonance integrals are defined with respect to the molecular orbitals: $t_{\mathrm{LUMO}}(\boldsymbol{l}) \equiv \langle\Psi_{\mathrm{LUMO}}(\boldsymbol{n})|\,\hat{H}\,|\Psi_{\mathrm{LUMO}}(\boldsymbol{n}+\boldsymbol{l})\rangle$ and $t_{\mathrm{HOMO}}(\boldsymbol{l}) \equiv \langle\Psi_{\mathrm{HOMO}}(\boldsymbol{n})|\,\hat{H}\,|\Psi_{\mathrm{HOMO}}(\boldsymbol{n}+\boldsymbol{l})\rangle$. The signs of $t_{\mathrm{LUMO}}(\boldsymbol{l})$ and $t_{\mathrm{HOMO}}(\boldsymbol{l})$ corresponding to transfer between two *nonequivalent* molecules depend on the chosen phase convention for the LUMOs and HOMOs. The phases are determined with the aid of a twofold screw rotation along the b-axis, located at $a/4$ and denoted as $\hat{S}_2$ (This is not a symmetry operation within the $P_{\bar{1}}$ space group of tetracene and pentacene, but nevertheless can be employed to define the phase based on a closely related monoclinic unit cell). Our convention is

$$phase(\psi_{\mathrm{LUMO},\beta}) = phase(\hat{S}_2\psi_{\mathrm{LUMO},\alpha});$$
$$phase(\psi_{\mathrm{HOMO},\beta}) = phase(\hat{S}_2\psi_{\mathrm{HOMO},\alpha}),$$

where α and β denote the two sub-lattices. The dissociation integrals corresponding to electron and hole transfer are presented in Table I for tetracene based on our B3LYP/DZ calculations. The values are in good agreement with those obtained by Tiberghien and Delacote.[46] The sign change between $t_{\mathrm{HOMO}}(\boldsymbol{l})$ and $t_{\mathrm{LUMO}}(\boldsymbol{l})$ (same sign for $D_e(\boldsymbol{l})$ and $D_h(\boldsymbol{l})$) along the diagonal ($\boldsymbol{l} = (\pm 1/2, \pm 1/2)$) directions is consistent with calculations of Hummer and Ambrosch-Draxl[47] which show crystalline tetracene to be a direct gap semiconductor along the diagonal directions. Note that we omit terms in H_{CT} which couple CT states to each other through $t_{\mathrm{HOMO}}(\boldsymbol{l})$ and $t_{\mathrm{LUMO}}(\boldsymbol{l})$. Such terms will induce splittings within the CT manifold, but such splittings are generally small compared to the Frenkel/CT gap prior to mixing ($\gtrsim$2000 cm^{-1}) and will therefore have minimal impact on the absorption spectrum. We also neglect the energy difference between the CT states with the electron and hole positions interchanged between the two sublattices. This is relevant only for triclinic tetracene and pentacene where the sublattices are nonequivalent.

The last term in Eq. (9) represents the coupling between the CT excitons and the symmetric molecular vibration and is given by

$$H_{CTV} = \omega_0 \sum_{\sigma,\boldsymbol{n}\in\sigma,l} \{\lambda_+(b_{\boldsymbol{n}}^\dagger + b_{\boldsymbol{n}}) + \lambda_-(b_{\boldsymbol{n}+\boldsymbol{l}}^\dagger + b_{\boldsymbol{n}+\boldsymbol{l}}) + \lambda_+^2 + \lambda_-^2\}|\boldsymbol{n},+;\ \boldsymbol{n}+\boldsymbol{l},-\rangle\langle\boldsymbol{n},+;\ \boldsymbol{n}+\boldsymbol{l},-|. \quad (12)$$

The Hamiltonian allows for independent anion and cation nuclear well shifts through the HR factors λ_+ and λ_-, respectively. Note that our model assumes all of the nuclear wells to be harmonic and of identical frequencies, ω_0. The cation HR factor for tetracene is estimated from the relative peak intensities in the vibronic progression present in the ultraviolet photoelectron spectrum of gas-phase tetracene.[44] From Ref. 44 we obtain $\lambda_+^2 \approx 0.32$. The anion HR factor was determined also in Ref. 44 based on DFT calculations yielding $\lambda_-^2 \approx 0.45$. (We find, however, that the absorption spectrum is fairly insensitive to the ionic HR factors. For example, doubling the ionic HR factors from the values reported above results in less than a 10% decrease of the DS.)

Within our enlarged basis set the αth eigenstate with wave vector $\boldsymbol{k}$ can be expanded as

$$|\Psi_{\alpha,\boldsymbol{k}}\rangle = \sum_\sigma \sum_{i=1,5} \sum_{\tilde{\nu}_i=0,1,\ldots 5} c_{i,\tilde{\nu}_i}^{\alpha,\boldsymbol{k}\sigma}\,|\boldsymbol{k}\sigma, i, \tilde{\nu}_i\rangle + \sum_\sigma \sum_{i=1,5} \sum_{\substack{\tilde{\nu}_i=0,1,\ldots 4\\ \nu=1,\ldots 4}} \sum_{\boldsymbol{l}} c_{i,\tilde{\nu}_i;\boldsymbol{l},\nu}^{\alpha,\boldsymbol{k}\sigma}\,|\boldsymbol{k}\sigma, i, \tilde{\nu}_i;\ \boldsymbol{l}, \nu\rangle + \sum_\sigma \sum_{\nu_-,\nu_+=0,1,\ldots 4} \sum_{\boldsymbol{l}} c_{\nu_+;\boldsymbol{l},\nu_-}^{\alpha,\boldsymbol{k}\sigma}\,|\boldsymbol{k}\sigma, \nu_+;\boldsymbol{l}, \nu_-\rangle\,. \quad (13)$$

In addition to the one- and two-particle excitons defined earlier in Eqs. (3) and (4), Eq. (13) also includes delocalized CT

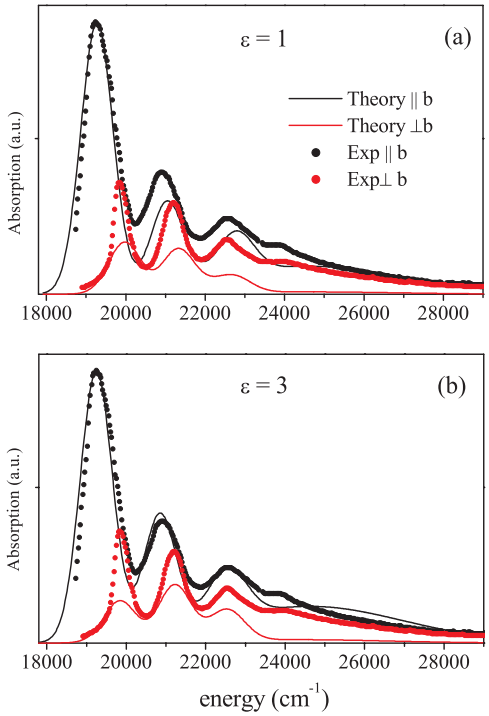

FIG. 4. Absorption spectra calculated on the basis of a model including both Frenkel and charge-transfer excitons alongside the measured spectra of Bree and Lyons (see Ref. 18). The optical dielectric constant is $\varepsilon = 1$ in (a) and $\varepsilon = 3$ in (b). Calculated spectra are spectrally shifted so that the *b*-polarized 0–0 peak frequency agrees with experiment (by adjusting $\Delta_{0\text{–}0}$); in addition, calculated spectra are normalized to the experimental 0–0 peak intensity for absorption along *b*.

excitons with wave vector $\boldsymbol{k}$ on sublattice σ,[35]

$$|\boldsymbol{k}\sigma, v_+; \boldsymbol{l}, v_-\rangle = \frac{1}{\sqrt{N_{cell}}} \sum_{\boldsymbol{n}\in\sigma} e^{i\boldsymbol{k}\cdot\boldsymbol{n}} |\boldsymbol{n}, v_+; \boldsymbol{n}+\boldsymbol{l}, v_-\rangle$$

$$\sigma = 1, 2. \quad (14)$$

Once expressed in the basis set defined above, we numerically diagonalized the Hamiltonian in Eq. (9) to determine all eigenstates and energies which were subsequently used to evaluate the absorption spectrum in Eq. (5) with the transition dipole moment operator defined in Eq. (6). Hence, we neglect the weak intrinsic transition dipole moment of the CT states. CT excitons gain oscillator strength only by mixing with Frenkel excitons.

Figures 4(a) and 4(b) display the calculated spectra for $\varepsilon = 1$ and $\varepsilon = 3$, respectively. The calculated spectra both agree well with experiment, although the agreement is clearly superior for the more realistic case using $\varepsilon = 3$. The comparison with experiment is summarized in Table II. The calculations capture the 0–0 DS quantitatively (+601 cm^{-1} vs. the measured value 631 cm^{-1}) as well as the 0–0/0–1 ratios, especially $A_{||b}^{0-0}/A_{||b}^{0-1}$. In fact, the calculations only disagree with experiment with respect to the polarization ratio, $A_{||b}^{0-0}/A_{\perp b}^{0-0}$, which is roughly 50% too high compared to experiment. This is most likely due to the anisotropy of the dielectric constant, which is neglected in present work.

The reversal in the ordering of the lowest excited states in the presence of CT excitons can be understood as follows.

TABLE II. Summary of calculated spectral characteristics of crystalline tetracene compared with the experimental values in Ref. 18. The polarization ratio (P.R.) is the ratio of the *b*-polarized to *a*-polarized 0–0 spectral areas. The CT contribution of the lower Davydov component of the 0–0 band is also shown. The DS are reported in cm^{-1}.

Tetracene	DS_{00}	DS_{01}	DS_{02}	P.R.	$\|b$ 00/01	$\perp b$ 00/01	CT (%)
Experiment (Ref. 18)	630	270	90	4.0	1.9	0.9	...
Theory: $\varepsilon = 1$	705	276	−172	5.2	2.9	1.1	28
Theory: $\varepsilon = 2$	629	343	−86	6.1	2.3	0.8	28
Theory: $\varepsilon = 3$	601	372	−38	6.4	2.1	0.7	27

As for the Frenkel excitons, the two sub-lattices give rise to symmetric and antisymmetric CT excitons that only couple to the Frenkel states of the same symmetry (we continue to assume a monoclinic unit cell for the sake of simplicity and ignore vibronic coupling). The coupling between symmetric (antisymmetric) states is given by $D_e + D_h$ ($D_e - D_h$), where D_e and D_h are the exciton dissociation integrals involving the movement of an elecron and hole, respectively, between nearest-neighbor (non-equivalent) molecules. When D_e and D_h have the same sign as in tetracene the interaction between symmetric states is much larger. Consequently, the *b*-polarized transition is pushed below the *a*-polarized transition resulting in a positive DS, in agreement with experiment. The mechanism is shown schematically in Fig. 5 for the simple case when $D_e = D_h$. The coupling between Frenkel and CT excitons also provides for an enhancement in the ratio, $A_{||b}^{0-0}/A_{||b}^{0-1}$, by roughly a factor of two, and a slight decrease in $A_{\perp b}^{0-0}/A_{\perp b}^{0-1}$, in excellent agreement with experiment. The movement of an electron and subsequently a hole between the two nearest-neighbor non-equivalent molecules effectively moves an excitation from one sublattice to the other. Our analysis shows that this second-order superexchange coupling is J-aggregate-like for the symmetric *b*-polarized exciton, thereby enhancing $A_{||b}^{0-0}/A_{||b}^{0-1}$, but is H-aggregate-like for the component polarized normal to *b*, accounting for the slight attenuation in $A_{\perp b}^{0-0}/A_{\perp b}^{0-1}$.[34] The near quantitative

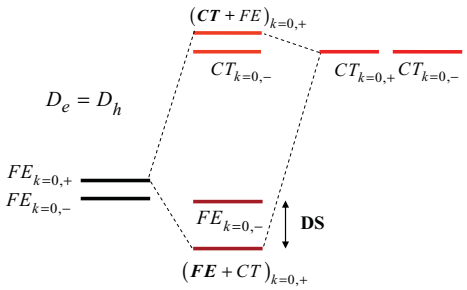

FIG. 5. Energy level diagram showing the interaction between Frenkel excitons on the left and CT excitons on the right in the simple case when $D_e = D_h$ for all four nearest neighbors. We also assume a monoclinic unit cell and no vibronic coupling. We take the interaction L_{12} (0) between sublattices to be small and positive (consistent with our detailed calculations in Sec. II) so that (before mixing) the symmetric (+) $\boldsymbol{k} = 0$, *b*-polarized exciton is slightly higher in energy than the antisymmetric (−) $\boldsymbol{k} = 0$, *a*-polarized exciton. Mixing with CT excitons of the same symmetry causes the symmetric exciton to be repelled below the antisymmetric exciton. This arises from a coupling matrix element proportional to $D_e + D_h$ in the symmetric case and $D_e - D_h$ (= 0) in the antisymmetric case.

TABLE III. CT state energies (in cm^{-1}) for anthracene and pentacene derived from the measured electroabsorption spectra (Refs. 24 and 25) relative to the lowest molecular exciton (S_1) energy. Also shown are the calculated dissociation integrals.

	Anthracene			Pentacene		
l	$\omega_{0-0}^{CT}(\boldsymbol{l}) - (\omega_{0-0}^{i=1} + \Delta_{0-0})$	$D_h(\boldsymbol{l})$	$D_e(\boldsymbol{l})$	$\omega_{0-0}^{CT}(\boldsymbol{l}) - (\omega_{0-0}^{i=1} + \Delta_{0-0})$	$D_h(\boldsymbol{l})$	$D_e(\boldsymbol{l})$
(1/2, 1/2)	x	201.7	540.4	x	− 381.5	− 665.4
(−1/2,1/2)	x	201.7	540.4	x	687.2	673.5
(0,1)	$x + 565$	387.2	313.8	$x + 1203$	− 272.6	− 347.6
(1,0)	$x + 1775$	− 0.6	5.6	$x + 1815$		
$x = 2390$ ($\varepsilon = 1$), 2662 ($\varepsilon = 2$), and 2737 ($\varepsilon = 3$)				$x = -250$ ($\varepsilon = 1$), 80 ($\varepsilon = 2$), and 160 ($\varepsilon = 3$)		

agreement with experiment leads to the conclusion that the Davydov splittings and relative vibronic peak intensities in crystalline triclinic tetracene are mainly due to Frenkel-CT coupling.

III. DAVYDOV SPLITTING IN ANTHRACENE AND PENTACENE

We also applied our analysis to anthracene and pentacene crystals, where we accounted for quantum-chemical interactions among the lowest Frenkel excitons, mixing with CT states, and coupling to high-frequency vibrations, in a way similar to the tetracene case. The parameters used to model the single molecule properties can be found in the Appendix (Table VI), while Table III gives the CT parameters for anthracene and pentacene, where the measured energy difference between the first CT state and the lowest (*b*-polarized) Frenkel exciton is respectively, 0.43 and 0.29 eV.[24,25] In addition, we have from Ref. 7 the values, ($\lambda_+^2 \approx 0.40$, $\lambda_-^2 \approx 0.58$) and ($\lambda_+^2 \approx 0.29$, $\lambda_-^2 \approx 0.39$), for anthracene and pentacene, respectively.

Figure 6 shows calculated polarized absorption spectra for anthracene crystals alongside the experimental spectra of Clark and Philpott.[16] Overall, the calculations adequately capture the relative band intensities and Davydov splittings. A comparison between theory and experiment is presented in Table IV.[16,17] Although the (0–0) DS of 270 cm^{-1} is somewhat larger than the value of ∼200 cm^{-1} reported in Refs. 16 and 17 it remains smaller than the value of 310 cm^{-1} reported in Ref. 48. The agreement with experiment may be slightly affected by our neglect of the dipole-forbidden MCD-detected B_{3u} state which, in anthracene, is only ≈ 2000 cm^{-1} above the S_1 state.[49]

For pentacene, the published spectra are difficult to analyze beyond the 0–0 DS, with the latter reported by several groups to be ∼1000–1100 cm^{-1}.[20,21] Table V summarizes the calculated and measured Davydov splittings in the oligoacene series, together with the CT contributions to the lower (0–0) Davydov component. The most striking result is the increased CT admixture with increasing oligoacene size: from a somewhat modest 10%–15% in anthracene (consistent with ealier claims[50] of weak mixing) to 25%–30% in tetracene, and to a very significant 45%–50% in pentacene. The increasing DS values correlate well with the increasing CT mixing and are in very good agreement with the experimental values. The evolution in Table V can be essentially traced back to the energy separation between the lowest Frenkel-like and CT-like electronic excitations in oligoacene crystals. Due to the increased size of the π-conjugated system and the resulting lower (higher) molecular ionization potential (electron affinity), this energy difference decreases from ∼0.4 eV in anthracene[24] to 0.29 eV in pentacene[25] (as extracted from electro-absorption experiments). As a result, stronger mixing

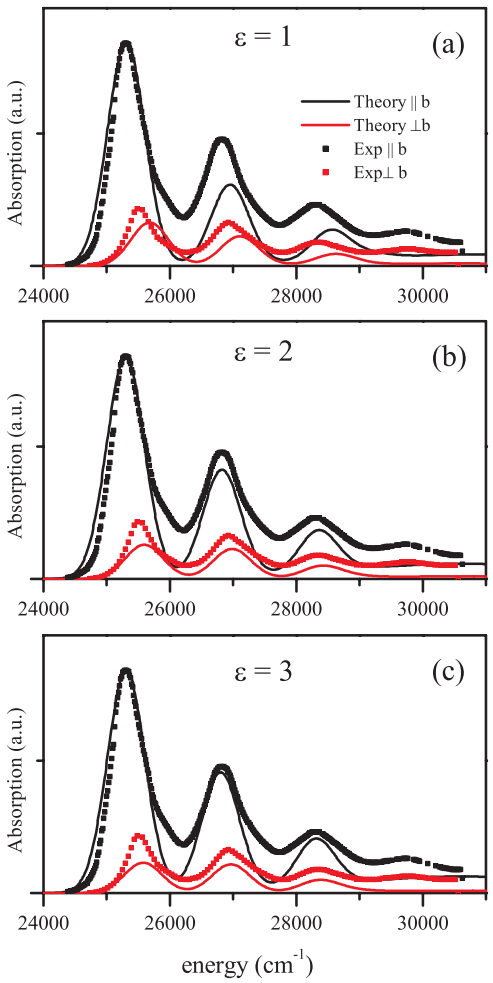

FIG. 6. Absorption spectra for crystalline antracene calculated on the basis of a model including both Frenkel and charge-transfer excitons alongside the experimental spectra of Clark and Philpott (see Ref. 16). Calculated spectra are spectrally shifted so that the *b*-polarized 0–0 peak frequency agrees with experiment (by adjusting Δ_{0-0}); in addition, calculated spectra are normalized to the experimental 0–0 peak intensity for absorption along *b*.

TABLE IV. Summary of calculated spectral characteristics of crystalline anthracene compared with the experimental values from Ref. 16. The polarization ratio (P.R.) is the ratio of the *b*-polarized to *a*-polarized 0–0 spectral areas. The CT contribution of the lower Davydov component of the 0–0 band is also shown. The DS are reported in cm^{-1}.

Anthracene	DS_{00}	DS_{01}	DS_{02}	P.R.	$\|b$ 00/01	$\perp b$ 00/01	CT (%)
Experiment (Ref. 16)	190	110	50	4.5	1.6	1.1	...
Theory: $\varepsilon = 1$	366	140	65	5.0	2.7	1.5	15
Theory: $\varepsilon = 2$	295	159	75	6.3	2.0	1.1	15
Theory: $\varepsilon = 3$	270	159	75	7.1	1.8	1.1	14

occurs between Frenkel and CT excitons in more extended oligoacenes, which consequently leads to larger DS values.

Improved results for pentacene, for which the Frenkel/CT gap prior to mixing is the smallest in the acene series, may require the inclusion of the neglected couplings *between* the various CT states. As stated earlier (see discussion in Subsection II B) neglect of such terms is justified when the Frenkel/CT gap prior to mixing significantly exceeds $|t_{\mathrm{HOMO}}(\boldsymbol{l})|$ and $|t_{\mathrm{LUMO}}(\boldsymbol{l})|$ which is easily satisfied for anthracene and tetracene. We are currently investigating the interactions between CT states across the acene series in an effort to account also for charge transport.

IV. IMPLICATIONS FOR EXCITON DISSOCIATION AND DIFFUSION

These results bear important implications regarding the fate of singlet excitons in the bulk of oligoacene crystals or thin films and at interfaces with electron acceptors. Exciton splitting to produce free charge carriers is obviously a key process in the operation of organic solar cells; it is generally considered to occur in two steps:[51] (i) photoinduced exciton dissociation into Coulombically bound charge-transfer pairs at donor/acceptor interfaces; and (ii) splitting of the bound electron-hole pairs into separated charge carriers. The second step involves the presence of local electric fields at the interface that can trigger charge separation over long distances and could be associated with the formation of interfacial dipoles.[52,53] Interestingly, the quantum yield for the generation of the precursor states involved in the first step can be expected to be maximized for large hybridization between Frenkel and CT excitons. Since we have shown that the DS in oligoacenes is a measure of the amount of CT admixture into the lowest excited states, it is therefore not surprising that the enhanced CT character of the lower Davydov component in

TABLE V. Summary of experimental vs. calculated 0–0 Davydov splittings (in cm^{-1}) in a series of oligoacenes. The CT contribution of the lower Davydov component of the 0–0 band is also shown. In all cases a dielectric constant of $\varepsilon = 3$ is taken.

	DS_{00} (expt.)	DS_{00} (theory)	CT (%)
Anthracene	190 (Ref. 16) 210 (Ref. 17)	270	14
Tetracene	630 (Ref. 18) 645 (Ref. 19)	601	27
Pentacene	1100 (Ref. 21) 1030 (Ref. 20)	1026	48

TABLE VI. Measured vibrational energies (ω_0) and molecular excited state energies (in cm^{-1}) for the oligoacenes considered in this work. The measured transition dipole moments (in Debye) and polarization directions (L = long axis, M = short axis) are shown alongside the energies. Calculated values are in parenthesis.

	ω_0	$\omega^1_{0-0}(S_1)$		$\omega^2_{0-0}(S_2)$		$\omega^3_{0-0}(S_3)$		$\omega^4_{0-0}(S_4)$		$\omega^5_{0-0}(S_5)$	
Anthracene (Refs. 22 and 63)	1400	26 000 (34 200)	2.93 (3.41) M	39 000 (40 572)	8.98 (9.96) L	44 500 (44 121)	3.07 (1.60) M	54 000 (45492)	3.99 (4.06) M	64 500 (56 704)	3.99 (2.74) M
Tetracene (Refs. 18 and 22)	1430	21 100 (29 764)	3.31 (3.65) M	34 000 (38 797)	2.50 (2.21) L	36 500 (37 023)	10.08 (11.79) L	44 000 (43637)	2.74 (1.57) M	47 500 (44 282)	4.37 (3.18) M
Pentacene (Refs. 22 and 64)	1350	17 100 (26 860)	3.51 (3.82) M	28 876 (34 119)	2.69 (3.91) L	32 990 (34 684)	12.49 (13.15) L	35 006 (42 992)	3.84 (3.35) M	43 960 (45 250)	3.36 (3.72) M

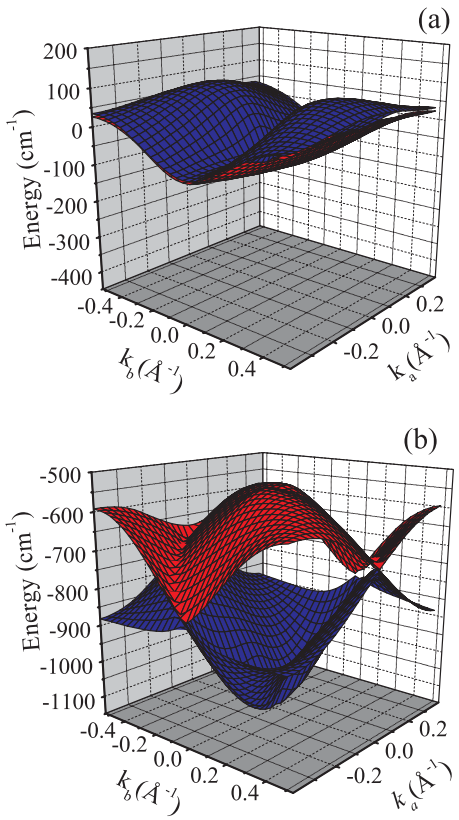

FIG. 7. Upper and lower 0–0 exciton bands calculated for a 300 × 300 tetracene herringbone aggregate in the *ab* plane. Only Frenkel one- and two-particle states are included in (a) while all Frenkel and CT states are included in (b). The blue (red) surface contains the k = 0 exciton responsible for absorption polarized mainly along *b* (*a*). The energies are reported relative to the single molecule S_1 exciton transition energy including the solution-to-crystal shift, $\omega_{0-0}^{(1)} + \Delta_{0-0}$. (The slight nonorthogonality between the directions of $\boldsymbol{k}_a$ and $\boldsymbol{k}_b$ – about 4° - cannot be noticed.)

pentacene translates into a high propensity for the excitons to split at the interface with C_{60}.

The admixture of Frenkel and CT excitons also leads to striking effects on the dispersion of the lower and upper exciton bands and, as a result, on the exciton diffusion rates. Figure 7 shows the calculated (0–0) upper and lower exciton bands in the *ab*-plane of tetracene without (Fig. 7(a)) and with (Fig. 7(b)) inclusion of CT states. In the absence of CT contributions, the lower and upper bands are almost superimposed, which leads to negligible DS. In addition, the $\boldsymbol{k} = 0$ exciton in the low energy band is *a*-polarized, in contrast to experiment. Admixing CT states reverses the order of the excitons near the band bottom (note, however, the avoided crossings for high wave vector excitons) and dramatically increases the DS value to 601 cm^{-1}, which differs from experiment by only 5%.

Figure 7 shows that the curvature near the lower band minimum is also greatly enhanced by the coupling between Frenkel and CT excitons; this results in higher exciton group velocities and, therefore, in higher diffusion coefficients. Under the constant-free-time approximation, appropriate for transport in the band limit, the exciton diffusion tensor is given by[54]

$$D_{ij} = \tau_{sc} \langle v_i v_j \rangle, \tag{15}$$

where $\langle v_i v_j \rangle$ is the thermally averaged velocity-velocity tensor and τ_{sc} is the isotropic relaxation (scattering) time; $\langle v_i v_j \rangle$ can be determined directly from the exciton dispersion curves as shown in Ref. 54. Based on this model, we calculate for tetracene at 200 K an isotropically averaged diffusion coefficient $\frac{1}{2}(D_{aa} + D_{bb})$ which increases by a factor of ≈ 6 when CT states are included. The enhancement derives entirely from $\langle v_i v_j \rangle$. If we consider a scattering time $\tau_{sc} \approx 15$ fs, as determined from recent photon-echo measurements on crystalline tetracene at 200 K,[55] we obtain $\frac{1}{2}(D_{aa} + D_{bb}) \approx 2 \times 10^{-2}$ cm^2/s. This value is in remarkable agreement with measured values of 4×10^{-2} cm^2/s (Ref. 56) and 0.7×10^{-2} cm^2/s (Ref. 57) based on an analysis of exciton-exciton annihilation and host-guest energy transfer, respectively. The band curvatures and hence the diffsusion coefficients in anthracene and pentacene are similarly enhanced by CT. However, as we are unaware of a consistent set of scattering times throughout the polyacene series, we cannot reliably compare calculated diffusion coefficients across the series.

V. CONCLUSION

In conclusion, our calculations based on one- and two-particle states in the five lowest Frenkel exciton bands along with all vibronic CT states deriving from the lowest (S_1) Frenkel exciton, are able to quantitatively reproduce the 0–0 Davydov splitting and relative 0-*n* vibronic intensities throughout a series of oligoacenes. The results demonstrate the increasing role played by CT contributions in going from anthracene to pentacene and provide a reliable basis to describe the connection between optical and transport properties in these technologically relevant materials. Specifically, the substantial contributions of charge-transfer configurations to the lowest electronic excitations of extended oligoacenes are predicted to: (i) facilitate exciton dissociation at donor/acceptor interfaces; and (ii) promote singlet exciton diffusion; both these processes are critical to the efficiency of organic solar cells. Finally, these findings are also key in understanding the important process of exciton fission in tetracene and pentacene, where CT states are believed to play an intermediate role.[58] Singlet fission may potentially double the production of charge carriers, which could have a beneficial impact on the efficiency of photovoltaic cells.[59]

ACKNOWLEDGMENTS

F.C.S. and H.Y. were supported by the National Science Foundation (NSF) under Award DMR-0906464. Work at Georgia Tech was partly supported by the Office of Naval Research (ONR), the STC Program of the National Science Foundation under Award DMR-0120967, and the Center for Advanced Molecular Photovoltaics, Award No KUSC1–015-21, made by King Abdullah University of Science and Technology (KAUST). Research in University of Mons was supported by the Interuniversity Attraction Pole program of the Belgian Federal Science Policy Office (PAI 6/27), Programme d'Excellence de la Région Wallonne (OPTI2MAT project), and FNRS-FRFC; D.B. is an FNRS Research Director. R.J.S. was supported as part of the Center for Excitonics, an Energy

Frontier Research Center funded by U.S. Department of Energy and Office of Science, Office of Basic Energy Science (Grant No. DE-SC0001088).

APPENDIX: SINGLE MOLECULE PARAMETERS

The molecular parameters describing the properties of isolated oliogoacene molecules are derived from the absorption spectra in solution. The transition energies, transition dipole moments, and polarizations for the first five singlet transitions, S_1–S_5 in anthracene, tetracene, and pentacene are reported in Table VI.

We also performed calculations to evaluate excited state energies and transition dipoles. The ground-state geometries of the oligoacenes were optimized using D_{2h} symmetry at the B3LYP/TZVP level of theory as implemented in TURBOMOLE version 5.9.[60] The singlet excited states at the B3LYP/TZVP optimized geometry were then characterized using the semi-empirical INDO (Ref. 61) method coupled with a CCSD (Ref. 62) electron correlation scheme using an active space composed of all the π molecular orbitals.

To ensure the transition energy and transition dipole moment were not strongly dependent on the size of the active space, additional INDO/CCSD calculations were performed using larger active spaces—up to 36 electrons in 36 orbitals in tetracene, for example. As the size of the active space increased, there were slight fluctuations in the transition energy but an overall trend toward convergence. The transition energy using the largest active space was within 0.1 eV of that calculated using only π orbitals. More importantly, the transition dipole moments demonstrated better convergence as the active space increased. For example, the S_1 transition dipole moments calculated using the two largest active spaces were less than 0.001 D of each other and the transition dipole moment calculated using only π orbitals was just 0.1 D larger than that calculated using the largest active space.

Table VI shows that the INDO/CCSD method overestimates the S_1 transition energy in all oligoacenes, due, in part, to the neglect of solvent-solute interactions. In contrast, calculated dipole moments are in much better agreement with the measured ones. Note that we have ordered the calculated transitions to best match the measured transition dipole moments. Hence, the calculated transition to S_3 in tetracene has slightly lower energy than the transition to S_2.

[1]M. Pope and C. E. Swenberg, *Electronic Processes in Organic Crystals and Polymers*, 2nd ed. (Oxford University Press, New York, 1999).
[2]E. A. Silinsh and V. Capek, *Organic Molecular Crystals: Interaction, Localization, and Transport Phenomena* (AIP, New York, 1994).
[3]V. M. Agranovich, *Excitations in Organic Solids* (Oxford University Press, New York, 2009).
[4]R. W. I. de Boer, M. E. Gershenson, A. F. Morpurgo, and V. Podzorov, Phys. Status Solidi A **201**, 1302 (2004).
[5]R. W. I. de Boer, M. Jochemsen, T. M. Klapwijk, A. F. Morpurgo, J. Niemax, A. K. Tripathi, and J. Pflaum, J. Appl. Phys. **95**, 1196 (2004).
[6]O. D. Jurchescu, J. Baas, and T. T. M. Palstra, Appl. Phys. Lett. **84**, 3061 (2004).
[7]V. Coropceanu, J. Cornil, D. A. da Silva, Y. Olivier, R. Silbey, and J. L. Bredas, Chem. Rev. **107**, 926 (2007).
[8]T. S. Ahn, A. M. Muller, R. O. Al-Kaysi, F. C. Spano, J. E. Norton, D. Beljonne, J. L. Bredas, and C. J. Bardeen, J. Chem. Phys. **128**, 054505 (2008).
[9]S.-H. Lim, T. G. Bjorklund, F. C. Spano, and C. J. Bardeen, Phys. Rev. Lett. **92**, 107402 (2004).
[10]M. Voigt, A. Langner, P. Schouwink, J. M. Lupton, R. F. Mahrt, and M. Sokolowski, J. Chem. Phys. **127**, 114705 (2007).
[11]A. Camposeo, M. Polo, S. Tavazzi, L. Silvestri, P. Spearman, R. Cingolani, and D. Pisignano, Phys. Rev. B **81**, 033306 (2010).
[12]J. J. Burdett, A. M. Muller, D. Gosztol, and C. J. Bardeen, J. Chem. Phys. **133**, 144506 (2010).
[13]S. Yoo, B. Domercq, and B. Kippelen, Appl. Phys. Lett. **85**, 5427 (2004).
[14]I. Salzmann, S. Duhm, R. Opitz, R. L. Johnson, J. P. Rabe, and N. Koch, J. Appl. Phys. **104**, 114518 (2008).
[15]A. S. Davydov, *Theory of Molecular Excitons* (Plenum, New York, 1971).
[16]L. B. Clark and M. R. Philpott, J. Chem. Phys. **53**, 3790 (1970).
[17]G. C. Morris and M. G. Sceats, Chem. Phys. **3**, 164 (1974).
[18]A. Bree and L. E. Lyons, J. Chem. Soc. 5206 (1960).
[19]S. Tavazzi, L. Raimondo, L. Silvestri, P. Spearman, A. Camposeo, M. Polo, and D. Pisignano, J. Chem. Phys. **128**, 154709 (2008).
[20]A. F. Prikhotko and L. I. Tsikora, Optics and Spectoscopy **25**, 242 (1968).
[21]V. Zanker and J. Preuss, Zeitschrift Fur Angewandte Physik **27**, 363 (1969).
[22]D. W. Schlosser and M. R. Philpott, Chem. Phys. **49**, 181 (1980).
[23]R. Schuster, M. Knupfer, and H. Berger, Phys. Rev. Lett. **98**, 037402 (2007).
[24]L. Sebastian, G. Weiser, G. Peter, and H. Bässler, Chem. Phys. **75**, 103 (1983).
[25]L. Sebastian, G. Weiser, and H. Bässler, Chem. Phys. **61**, 125 (1981).
[26]Q. X. Yang, M. Muntwiler, and X. Y. Zhu, Phys. Rev. B **80**, 115214 (2009).
[27]X. Y. Zhu, Q. Yang, and M. Muntwiler, Acc. Chem. Res. **42**, 1779 (2009).
[28]B. Petelenz, P. Petelenz, H. F. Shurvell, and V. H. Smith, Chem. Phys. **119**, 25 (1988).
[29]M. L. Tiago, J. E. Northrup, and S. G. Louie, Phys Rev. B **67**, 115212 (2003).
[30]Subsequent work by Petelenz and co-workers have included vibronic coupling in the strong coupling approximation to evaluate electroabsorption spectra of oligoacene crystals, see P. Petelenz, M. Slawik, K. Yokoi, and M. Z. Zgierski, J. Chem. Phys. **105**, 4427 (1996).
[31]M. R. Philpott, J. Chem. Phys. **55**, 2039 (1971).
[32]F. C. Spano, J. Chem. Phys. **116**, 5877 (2002).
[33]F. C. Spano, Annu. Rev. Phys. Chem. **57**, 217 (2006).
[34]F. C. Spano, Acc. Chem. Res. **43**, 429 (2010).
[35]M. Hoffmann and Z. G. Soos, Phys. Rev. B **66**, 024305 (2002).
[36]A. Stradomska and P. Petelenz, J. Chem. Phys. **131**, 044507 (2009).
[37]J. L. Bredas, D. Beljonne, V. Coropceanu, and J. Cornil, Chem. Rev. **104**, 4971 (2004).
[38]B. P. Krueger, G. D. Scholes, and G. R. Fleming, J. Phys. Chem. B **102**, 5378 (1998).
[39]D. Beljonne, J. Cornil, R. Silbey, P. Millie, and J. L. Bredas, J. Chem. Phys. **112**, 4749 (2000).
[40]F. C. Spano, S. C. J. Meskers, E. Hennebicq, and D. Beljonne, J. Am. Chem. Soc. **129**, 7044 (2007).
[41]M. R. Philpott, J. Chem. Phys. **58**, 588 (1973).
[42]T. Sakurai and S. Hayakawa, Jpn. J. Appl. Phys. **13**, 1733 (1974).
[43]H. Yamagata, unpublished results.
[44]V. Coropceanu, M. Malagoli, D. A. da Silva, N. E. Gruhn, T. G. Bill, and J. L. Bredas, Phys. Rev. Lett. **89**, 275503 (2002).
[45]P. J. Bounds and W. Siebrand, Chem. Phys. Lett. **75**, 414 (1980).
[46]A. Tiberghien and G. Delacote, Chem. Phys. Lett. **8**, 88 (1971).
[47]K. Hummer and C. Ambrosch-Draxl, Phys Rev. B **72**, 205205 (2005).
[48]A. Matsui, J. Phys. Soc. Jpn. **21**, 2212 (1966).
[49]R. P. Steiner and J. Michl, J. Am. Chem. Soc. **100**, 6861 (1978).
[50]R. Silbey, J. Jortner, and S. A. Rice, J. Chem. Phys. **42**, 1515 (1965).
[51]J.-L. Bredas, J. E. Norton, J. Cornil, and V. Coropceanu, Acc. Chem. Res. **42**, 1691 (2009).
[52]T. M. Clarke and J. R. Durrant, Chem. Rev. **110**, 6736 (2010).
[53]S. Verlaak, D. Beljonne, D. Cheyns, C. Rolin, M. Linares, F. Castet, J. Cornil, and P. Heremans, Adv. Funct. Mater. **19**, 3809 (2009).
[54]Y. C. Cheng, R. J. Silbey, D. A. da Silva, J. P. Calbert, J. Cornil, and J. L. Bredas, J. Chem. Phys. **118**, 3764 (2003).
[55]B. A. West, J. M. Womick, L. E. McNeil, K. J. Tan, and A. M. Moran, J. Phys. Chem. C **114**, 10580 (2010).

[56]A. J. Campillo, R. C. Hyer, S. L. Shapiro, and C. E. Swenberg, Chem. Phys. Lett. **48**, 495 (1977).
[57]A. J. Campillo, S. L. Shapiro, and C. E. Swenberg, Chem. Phys. Lett. **52**, 11–15 (1977).
[58]E. C. Greyson, J. Vura-Weis, J. Michl, and M. A. Ratner, J. Phys. Chem B **114**, 14168 (2010).
[59]A. Rao, M. W. B. Wilson, J. M. Hodgkiss, S. Albert-Seifried, H. Bässler, and R. H. Friend, J. Am. Chem. Soc. **132**, 12698 (2010).
[60]R. Ahlrichs, M. Bar, M. Haser, H. Horn, and C. Kolmel, Chem. Phys. Lett. **162**, 165 (1989).
[61]J. Ridley and M. Zerner, Theor. Chem. Acc. **32**, 111 (1973).
[62]S. Hirata, M. Nooijen, and R. J. Bartlett, Chem. Phys. Lett. **326**, 255 (2000).
[63]M. R. Philpott, J. Chem. Phys. **59**, 4406 (1973).
[64]C. Hellner, P. C. Roberge, and Lindqvis L., J. Chem. Soc., Faraday Trans. **68**, 1928 (1972).